J Wood Sci (2016) 62:29–41
DOI 10.1007/s10086-015-1524-5

ORIGINAL ARTICLE

A general solution technique for electroelastic fields in piezoelectric bodies with D_∞ symmetry in cylindrical coordinates

Masayuki Ishihara[1] · Yoshihiro Ootao[1] · Yoshitaka Kameo[2]

Received: 2 September 2015 / Accepted: 19 October 2015 / Published online: 18 January 2016

Abstract To elucidate the electroelastic field in bodies with D_∞ symmetry such as wooden materials, we constructed a general solution technique for electroelastic problems in such bodies in a cylindrical coordinate system. We introduced the displacement and electric potential functions to express the displacement and electric field in cylindrical coordinates; their governing equations were obtained using the fundamental equations for the electroelastic field. The electroelastic field quantities could be expressed in terms of two elastic displacement potential functions and two piezoelastic displacement potential functions, each of which satisfies a Laplace equation with respect to the appropriately transformed cylindrical coordinates. As an application of the technique, we analyzed the problem of an infinitely long cylinder subjected to a non-axisymmetrically distributed electric surface potential. Using numerical calculations, we elucidated the electroelastic field quantities within the cylinder and found unique electroelastic coupling behaviors, which clearly demonstrate the necessity for the analytical technique presented. Moreover, we confirmed the possibility of the nondestructive evaluation (NDE) techniques by use of the piezoelectric effects.

Keywords Piezoelectric body · D_∞ symmetry · Electroelasticity · General solution technique · Cylindrical scheme

✉ Masayuki Ishihara
ishihara@me.osakafu-u.ac.jp

[1] Graduate School of Engineering, Osaka Prefecture University, 1-1 Gakuen-cho, Naka-ku, Sakai 599-8531, Japan

[2] Institute for Frontier Medical Sciences, Kyoto University, 53, Kawahara-cho, Shogoin, Sakyo-ku, Kyoto 606-8507, Japan

Introduction

Green materials have attracted considerable attention recently due to increasing demands for reduction in environmental loads. Two of the more desired properties of green materials are biodegradability and carbon-neutrality. From an engineering viewpoint, wood is one of the most promising materials to achieve these properties. Wood exhibits piezoelectricity [1], and has been the subject of electroelastic problems aimed at developing nondestructive evaluation (NDE) techniques to ensure the quality of wooden materials [2–9].

Because wood is composed of complicated microstructures, investigations from a microscopic approach were made [10–14]. In the design procedures of engineering applications, however, a macroscopic approach is required in order to avoid a considerably high computational cost associated with a microscopic approach. From such a viewpoint, wood is considered to have a D_∞ macrosymmetry, characterized by an ∞-fold rotation axis with a perpendicular two-fold rotation axis [15], although it is generally recognized as an orthotropic material when considering the effects of annual rings [14, 16]. Briefly speaking, D_∞ symmetry develops as a result of uniaxial and random aggregation of constituent molecular chains [1, 9]. Bodies with D_∞ symmetry exhibit a unique electroelastic coupling behavior: coupling only occurs between the electric poling perpendicular to the ∞-fold rotation axis and the shear motion in the plane perpendicular to the poling, as shown in Fig. 1.

Safe use of wood in engineering applications requires analytical solutions of the relevant electroelastic problems because few tools can reveal the field quantities within bodies. Motivated by this idea, we obtained analytical solutions for semi-infinite bodies with D_∞ symmetry

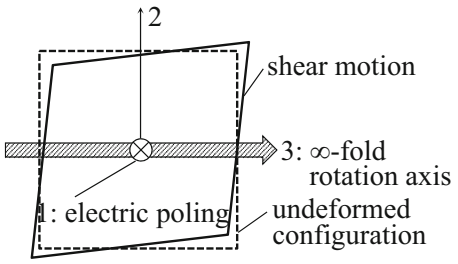

Fig. 1 Electroelastic coupling in a body with D_∞ symmetry

subjected to electric [17] or mechanical loading [18]. Successfully solving these electroelastic problems in semi-infinite bodies [17, 18] relied on using the Cartesian coordinate system framework. In many engineering applications, however, the problems must be handled in terms of cylindrical coordinates. For example, cylindrical columns of wood are common, and material defects—such as cracks, voids, knots, and pith—are often cylindrical. Consequently, it is absolutely essential not only to solve a specific problem but also to construct a general solution scheme that can handle various problems in cylindrical coordinates.

In this paper, therefore, we construct a general solution technique for electroelastic problems in bodies with D_∞ symmetry under the framework of a cylindrical coordinate system. First, the cylindrical components of displacement and electric field are expressed in terms of two types of displacement potential functions and the electric potential function. Then, the governing equations for these potential functions are obtained by applying the equilibrium of stresses and Gauss's law. As a result, the electric potential function and the cylindrical components of the displacement, strain, stress, electric field, and electric displacement are expressed in terms of four functions: two elastic displacement potential functions and two piezoelastic displacement potential functions, each of which satisfies a Laplace equation with respect to the cylindrical coordinates transformed by the material properties. We apply the technique to one of the most elementary models of an NDE by use of the piezoelectric effects, in which a cylindrical body is exposed to the electric field across the longitudinal axis of the body, and illustrate the results graphically.

General solution technique

Fundamental equations

We consider a body with D_∞ symmetry. A cylindrical coordinate system (r, θ, z) is defined such that the z-axis is parallel to the ∞-fold rotation axis of the body. The constitutive equations in the isothermal case are [17]

$$\begin{Bmatrix}\sigma_{rr}\\ \sigma_{\theta\theta}\\ \sigma_{zz}\\ \sigma_{\theta z}\\ \sigma_{zr}\\ \sigma_{r\theta}\end{Bmatrix} = \begin{bmatrix} c_{11} & c_{12} & c_{13} & 0 & 0 & 0\\ & c_{11} & c_{13} & 0 & 0 & 0\\ & & c_{33} & 0 & 0 & 0\\ & & & c_{44} & 0 & 0\\ & & & & c_{44} & 0\\ \text{sym.} & & & & & \frac{c_{11}-c_{12}}{2}\end{bmatrix}\begin{Bmatrix}\varepsilon_{rr}\\ \varepsilon_{\theta\theta}\\ \varepsilon_{zz}\\ 2\varepsilon_{\theta z}\\ 2\varepsilon_{zr}\\ 2\varepsilon_{r\theta}\end{Bmatrix} - \begin{bmatrix} 0 & 0 & 0\\ 0 & 0 & 0\\ 0 & 0 & 0\\ e_{14} & 0 & 0\\ 0 & -e_{14} & 0\\ 0 & 0 & 0\end{bmatrix}\begin{Bmatrix}E_r\\ E_\theta\\ E_z\end{Bmatrix}, \tag{1}$$

$$\begin{Bmatrix}D_r\\ D_\theta\\ D_z\end{Bmatrix} = \begin{bmatrix} 0 & 0 & 0 & e_{14} & 0 & 0\\ 0 & 0 & 0 & 0 & -e_{14} & 0\\ 0 & 0 & 0 & 0 & 0 & 0\end{bmatrix}\begin{Bmatrix}\varepsilon_{rr}\\ \varepsilon_{\theta\theta}\\ \varepsilon_{zz}\\ 2\varepsilon_{\theta z}\\ 2\varepsilon_{zr}\\ 2\varepsilon_{r\theta}\end{Bmatrix} + \begin{bmatrix} \eta_{11} & 0 & 0\\ & \eta_{11} & 0\\ \text{sym.} & & \eta_{33}\end{bmatrix}\begin{Bmatrix}E_r\\ E_\theta\\ E_z\end{Bmatrix}, \tag{2}$$

where $(\varepsilon_{rr}, \varepsilon_{\theta\theta}, \varepsilon_{zz}, \varepsilon_{\theta z}, \varepsilon_{zr}, \varepsilon_{r\theta})$, $(\sigma_{rr}, \sigma_{\theta\theta}, \sigma_{zz}, \sigma_{\theta z}, \sigma_{zr}, \sigma_{r\theta})$, (E_r, E_θ, E_z), and (D_r, D_θ, D_z) denote the components of the strain, stress, electric field, and electric displacement, respectively, in the cylindrical coordinate system; c_{ij}, η_{kl}, and e_{kj} denote the elastic stiffness constant, dielectric constant, and piezoelectric constant, respectively. Only the piezoelectric constant e_{14} couples the electric field or the electric displacement perpendicular to the ∞-fold rotation axis (z-axis) with the strain or stress in the plane perpendicular to the electric field or electric displacement.

The displacement–strain relations, stress equilibrium equations, and Gauss's law are:

$$\left.\begin{aligned} &\varepsilon_{rr} = \frac{\partial u_r}{\partial r},\ \varepsilon_{\theta\theta} = \frac{u_r}{r} + \frac{1}{r}\frac{\partial u_\theta}{\partial \theta},\ \varepsilon_{zz} = \frac{\partial u_z}{\partial z},\\ &2\varepsilon_{\theta z} = \frac{\partial u_\theta}{\partial z} + \frac{1}{r}\frac{\partial u_z}{\partial \theta},\ 2\varepsilon_{zr} = \frac{\partial u_z}{\partial r} + \frac{\partial u_r}{\partial z},\ 2\varepsilon_{r\theta} = \frac{1}{r}\frac{\partial u_r}{\partial \theta} + \frac{\partial u_\theta}{\partial r} - \frac{u_\theta}{r}\end{aligned}\right\}, \tag{3}$$

$$\left.\begin{aligned} &\frac{\partial \sigma_{rr}}{\partial r} + \frac{1}{r}\frac{\partial \sigma_{r\theta}}{\partial \theta} + \frac{\partial \sigma_{zr}}{\partial z} + \frac{\sigma_{rr} - \sigma_{\theta\theta}}{r} = 0,\\ &\frac{\partial \sigma_{r\theta}}{\partial r} + \frac{1}{r}\frac{\partial \sigma_{\theta\theta}}{\partial \theta} + \frac{\partial \sigma_{\theta z}}{\partial z} + 2\frac{\sigma_{r\theta}}{r} = 0,\\ &\frac{\partial \sigma_{zr}}{\partial r} + \frac{1}{r}\frac{\partial \sigma_{\theta z}}{\partial \theta} + \frac{\partial \sigma_{zz}}{\partial z} + \frac{\sigma_{zr}}{r} = 0\end{aligned}\right\}, \tag{4}$$

$$\frac{\partial D_r}{\partial r} + \frac{D_r}{r} + \frac{1}{r}\frac{\partial D_\theta}{\partial \theta} + \frac{\partial D_z}{\partial z} = 0, \tag{5}$$

respectively, where (u_r, u_θ, u_z) denotes the displacement in cylindrical coordinates.

Governing equations for the potential functions

We introduce the displacement potential functions φ and ϑ as:

$$u_r = \frac{\partial \varphi}{\partial r} + \frac{1}{r}\frac{\partial \vartheta}{\partial \theta},\ u_\theta = \frac{1}{r}\frac{\partial \varphi}{\partial \theta} - \frac{\partial \vartheta}{\partial r},\ u_z = k\frac{\partial \varphi}{\partial z}, \tag{6}$$

where k is an as-yet unknown constant. The components of the electric field are expressed in terms of the electric potential function Φ as:

$$E_r = -\frac{\partial \Phi}{\partial r},\ E_\theta = -\frac{1}{r}\frac{\partial \Phi}{\partial \theta},\ E_z = -\frac{\partial \Phi}{\partial z}. \tag{7}$$

Substituting Eqs. (3), (6), and (7) into Eqs. (1) and (2), which are then substituted into Eqs. (4) and (5), we have

$$\left\{c_{11}\left(\frac{\partial^2}{\partial r^2} + \frac{1}{r}\frac{\partial}{\partial r} + \frac{1}{r^2}\frac{\partial^2}{\partial \theta^2}\right) + [kc_{13} + (1+k)c_{44}]\frac{\partial^2}{\partial z^2}\right\}\varphi = 0, \tag{8}$$

$$\left\{[c_{13} + (1+k)c_{44}]\left(\frac{\partial^2}{\partial r^2} + \frac{1}{r}\frac{\partial}{\partial r} + \frac{1}{r^2}\frac{\partial^2}{\partial \theta^2}\right) + kc_{33}\frac{\partial^2}{\partial z^2}\right\}\varphi = 0, \tag{9}$$

$$\left[\frac{c_{11} - c_{12}}{2}\left(\frac{\partial^2}{\partial r^2} + \frac{1}{r}\frac{\partial}{\partial r} + \frac{1}{r^2}\frac{\partial^2}{\partial \theta^2}\right) + c_{44}\frac{\partial^2}{\partial z^2}\right]\vartheta - e_{14}\frac{\partial \Phi}{\partial z} = 0, \tag{10}$$

$$e_{14}\frac{\partial}{\partial z}\left(\frac{\partial^2}{\partial r^2} + \frac{1}{r}\frac{\partial}{\partial r} + \frac{1}{r^2}\frac{\partial^2}{\partial \theta^2}\right)\vartheta + \left[\eta_{11}\left(\frac{\partial^2}{\partial r^2} + \frac{1}{r}\frac{\partial}{\partial r} + \frac{1}{r^2}\frac{\partial^2}{\partial \theta^2}\right) + \eta_{33}\frac{\partial^2}{\partial z^2}\right]\Phi = 0. \tag{11}$$

Since the governing equations for φ, Eqs. (8) and (9), should be identical,

$$\frac{kc_{13} + (1+k)c_{44}}{c_{11}} = \frac{kc_{33}}{c_{13} + (1+k)c_{44}} \equiv \mu. \tag{12}$$

Solving Eq. (12) for k gives

$$k = \frac{c_{11}\mu - c_{44}}{c_{13} + c_{44}} = \frac{(c_{13} + c_{44})\mu}{c_{33} - c_{44}\mu}, \tag{13}$$

which leads to a quadratic equation for μ:

$$c_{11}c_{44}\mu^2 - (c_{11}c_{33} - c_{13}^2 - 2c_{13}c_{44})\mu + c_{33}c_{44} = 0. \tag{14}$$

For μ satisfying Eq. (14), Eqs. (8) and (9) both become

$$\left(\frac{\partial^2}{\partial r^2} + \frac{1}{r}\frac{\partial}{\partial r} + \frac{1}{r^2}\frac{\partial^2}{\partial \theta^2} + \mu\frac{\partial^2}{\partial z^2}\right)\varphi = 0. \tag{15}$$

From Eqs. (10), (11), and (15), the governing equation of φ is not coupled with the electric potential function Φ, whereas the displacement potential function ϑ is coupled with Φ through the piezoelectric constant e_{14}. Associated with these characteristics, we hereafter refer to φ as an elastic displacement potential function and ϑ as a piezoelastic displacement potential function, respectively.

Governing equation for the elastic displacement potential function

We denote the two roots of the quadratic Eq. (14) as μ_1 and μ_2, the corresponding φ as φ_1 and φ_2, and the corresponding k as k_1 and k_2, respectively. Then, from Eq. (15), the governing equations for φ_1 and φ_2 are

$$\left(\frac{\partial^2}{\partial r^2} + \frac{1}{r}\frac{\partial}{\partial r} + \frac{1}{r^2}\frac{\partial^2}{\partial \theta^2} + \mu_i\frac{\partial^2}{\partial z^2}\right)\varphi_i = 0,\quad (i = 1, 2). \tag{16}$$

From Eq. (13),

$$k_i = \frac{c_{11}\mu_i - c_{44}}{c_{13} + c_{44}} = \frac{(c_{13} + c_{44})\mu_i}{c_{33} - c_{44}\mu_i},\quad (i = 1,\ 2). \tag{17}$$

Hereafter, we consider the case that μ_1 and μ_2 are different positive numbers.

Governing equation for the piezoelastic displacement potential function

Eliminating Φ from Eqs. (10) and (11) results in

$$\left\{\left(\frac{\partial^2}{\partial r^2} + \frac{1}{r}\frac{\partial}{\partial r} + \frac{1}{r^2}\frac{\partial^2}{\partial \theta^2}\right)^2 + \left[\mu_3\left(1 + k_{\text{couple}}^2\right) + \eta\right]\left(\frac{\partial^2}{\partial r^2} + \frac{1}{r}\frac{\partial}{\partial r} + \frac{1}{r^2}\frac{\partial^2}{\partial \theta^2}\right)\frac{\partial^2}{\partial z^2} + \mu_3\eta\frac{\partial^4}{\partial z^4}\right\}\vartheta = 0, \tag{18}$$

where

$$\mu_3 = \frac{2c_{44}}{c_{11} - c_{12}},\ \eta = \frac{\eta_{33}}{\eta_{11}},\ k_{\text{couple}} = \frac{e_{14}}{\sqrt{c_{44}\eta_{11}}}. \tag{19}$$

Furthermore, the differential operator in Eq. (18) can be factorized as

$$\left(\frac{\partial^2}{\partial r^2} + \frac{1}{r}\frac{\partial}{\partial r} + \frac{1}{r^2}\frac{\partial^2}{\partial \theta^2} + \upsilon_1\frac{\partial^2}{\partial z^2}\right)\left(\frac{\partial^2}{\partial r^2} + \frac{1}{r}\frac{\partial}{\partial r} + \frac{1}{r^2}\frac{\partial^2}{\partial \theta^2} + \upsilon_2\frac{\partial^2}{\partial z^2}\right)\vartheta = 0, \tag{20}$$

where υ_1 and υ_2 denote two roots of a quadratic equation for υ:

$$\upsilon^2 - \left[\mu_3\left(1 + k_{\text{couple}}^2\right) + \eta\right]\upsilon + \mu_3\eta = 0. \tag{21}$$

Since υ_1 and υ_2 are different positive numbers [17], a general solution to Eq. (20) is

$$\vartheta = \vartheta_1 + \vartheta_2, \tag{22}$$

where ϑ_1 and ϑ_2 denote the general solutions to

$$\left(\frac{\partial^2}{\partial r^2} + \frac{1}{r}\frac{\partial}{\partial r} + \frac{1}{r^2}\frac{\partial^2}{\partial \theta^2} + \upsilon_i \frac{\partial^2}{\partial z^2}\right)\vartheta_i = 0, \quad (i = 1,\ 2). \tag{23}$$

By substituting ϑ of Eqs. (21)–(23) into Eq. (10) and integrating with respect to z, we can solve for Φ.

General solution of the electroelastic field

The governing equations for φ_i and ϑ_i, Eqs. (16) and (23), are the Laplace equations in coordinates $\left(r,\ \theta,\ z/\sqrt{\mu_i}\right)$ and $\left(r,\ \theta,\ z/\sqrt{\upsilon_i}\right)$, respectively, for which general solutions are well established. By substituting the general solutions for φ_i and ϑ_i (i =1, 2), and the electric potential function Φ as solved in the previous subsection into Eqs. (6) and (7), and then substituting the results into Eq. (3), we arrive at general solutions for the components of the displacement, electric field, and strain in cylindrical coordinates,

$$\begin{aligned} u_r &= \sum_{i=1}^{2}\left(\frac{\partial \varphi_i}{\partial r} + \frac{1}{r}\frac{\partial \vartheta_i}{\partial \theta}\right),\ u_\theta = \sum_{i=1}^{2}\left(\frac{1}{r}\frac{\partial \varphi_i}{\partial \theta} - \frac{\partial \vartheta_i}{\partial r}\right), \\ u_z &= \frac{\partial}{\partial z}\sum_{i=1}^{2} k_i \varphi_i, \end{aligned} \tag{24}$$

$$E_r = -\frac{\partial \Phi}{\partial r},\ E_\theta = -\frac{1}{r}\frac{\partial \Phi}{\partial \theta},\ E_z = -\frac{\partial \Phi}{\partial z}, \tag{25}$$

$$\left.\begin{aligned} \varepsilon_{rr} &= \sum_{i=1}^{2}\left(\frac{\partial^2 \varphi_i}{\partial r^2} + \frac{1}{r}\frac{\partial^2 \vartheta_i}{\partial r \partial \theta} - \frac{1}{r^2}\frac{\partial \vartheta_i}{\partial \theta}\right),\ \varepsilon_{\theta\theta} = \sum_{i=1}^{2}\left(\frac{1}{r}\frac{\partial \varphi_i}{\partial r} + \frac{1}{r^2}\frac{\partial^2 \varphi_i}{\partial \theta^2} - \frac{1}{r}\frac{\partial^2 \vartheta_i}{\partial r \partial \theta} + \frac{1}{r^2}\frac{\partial \vartheta_i}{\partial \theta}\right), \\ \varepsilon_{zz} &= \sum_{i=1}^{2} k_i \frac{\partial^2 \varphi_i}{\partial z^2},\ 2\varepsilon_{\theta z} = \sum_{i=1}^{2}\left[(1+k_i)\frac{1}{r}\frac{\partial^2 \varphi_i}{\partial \theta \partial z} - \frac{\partial^2 \vartheta_i}{\partial r \partial z}\right],\ 2\varepsilon_{zr} = \sum_{i=1}^{2}\left[(1+k_i)\frac{\partial^2 \varphi_i}{\partial r \partial z} + \frac{1}{r}\frac{\partial^2 \vartheta_i}{\partial \theta \partial z}\right], \\ 2\varepsilon_{r\theta} &= \sum_{i=1}^{2}\left(\frac{2}{r}\frac{\partial^2 \varphi_i}{\partial r \partial \theta} - \frac{2}{r^2}\frac{\partial \varphi_i}{\partial \theta} - \frac{\partial^2 \vartheta_i}{\partial r^2} + \frac{1}{r}\frac{\partial \vartheta_i}{\partial r} + \frac{1}{r^2}\frac{\partial^2 \vartheta_i}{\partial \theta^2}\right) \end{aligned}\right\}, \tag{26}$$

respectively. We can also obtain the components of stress by substituting Eqs. (25) and (26) into Eq. (1) and the electric displacement components by substituting Eqs. (25) and (26) into Eq. (2).

Application to infinitely long cylinder subjected to electric field

We apply the general solution technique presented in the previous section to a concrete boundary-value problem to verify the validity of the proposed technique. As an analytical model, we consider an infinitely long cylinder of radius R with D_∞ symmetry, oriented such that the z-axis parallels the ∞-fold rotation axis of the body, as shown in Fig. 2. The surface of the cylinder experiences no stresses and is subjected to the electric potential distribution

$$(\Phi)_{r=R} = \Phi_0 \sin\theta \times \exp\left(-\frac{z^2}{\delta^2}\right), \tag{27}$$

where Φ_0 and δ denote the characteristic value of the electric potential and the effective width of the distribution along the z-axis, respectively. Equation (27) is periodic with fundamental period 2π with respect to θ, symmetric with respect to $x = 0$ and $z = 0$, and anti-symmetric with respect to $y = 0$. The stresses and electric fields are assumed to vanish at infinity.

This is one of the most fundamental models of an NDE by use of the piezoelectric effects. When a body undergoes such an evaluation, a local electric field is applied to the body through electrodes. The distribution defined by Eq. (27) is intended to model electric potentials of $\pm\Phi_0$ around the points $(\theta, z) = (\pm\pi/2, 0)$, respectively. Strictly speaking, the electric potentials should be defined to be uniform on certain bounded regions around those points. Equation (27), which prescribes the nonuniform distribution over the entire surface, is introduced as a first step to treat the problem analytically, and simplifies the following mathematical procedures. Moreover, the model free from material defects is chosen because its behavior is required as a reference state in NDE techniques.

Analysis

We apply boundary conditions,

$$r = R: \ \sigma_{rr} = 0, \ \sigma_{r\theta} = 0, \ \sigma_{zr} = 0,$$
$$\Phi = \Phi_0 \sin\theta \times \exp\left(-\frac{z^2}{\delta^2}\right) \tag{28}$$

to our infinite cylinder.

Considering the periodicity, symmetry, and finiteness of the electroelastic field, as discussed above, the general solutions to Eqs. (16) and (23) become [19]

$$\varphi_i = \int_0^\infty A_i(\alpha) I_1\left(\sqrt{\mu_i}\alpha r\right) \sin(\alpha z)\mathrm{d}\alpha \times \cos\theta, \tag{29}$$

$$\vartheta_i = \int_0^\infty C_i(\alpha) I_1\left(\sqrt{\upsilon_i}\alpha r\right) \sin(\alpha z)\mathrm{d}\alpha \times \sin\theta, \tag{30}$$

where $I_n()$ denotes the modified Bessel function of the first kind of order n and $A_i(\alpha)$ and $C_i(\alpha)$, (i =1, 2) are unknown constants to be determined from the boundary conditions described by Eq. (28). The single-term expressions with respect to θ in Eqs. (29) and (30) are conceived from the nature of distribution described by the last equation in Eq. (28). For a practical distribution with θ such as partially uniform one, the single-term expression in Eq. (28) is replaced with the Fourier series with respect to θ, and therefore the solutions for φ_i and ϑ_i are obtained by replacing the single-term expressions in Eqs. (29) and (30) with the corresponding series expressions, which suggests the versatility of our methodology.

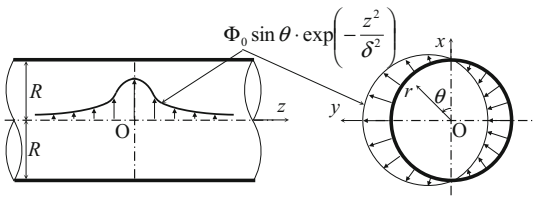

Fig. 2 Analytical model

Furthermore, we substitute Eq. (30) into Eqs. (10) and (22) and integrate the result with respect to z, arriving at the general solution of the electric potential function

$$\Phi = -\frac{c_{44}}{e_{14}\mu_3}\sum_{i=1}^{2}\int_0^\infty (\upsilon_i - \mu_3)\alpha C_i(\alpha) I_1\left(\sqrt{\upsilon_i}\alpha r\right)\cos(\alpha z)\mathrm{d}\alpha \times \sin\theta. \tag{31}$$

Substituting Eqs. (29)–(31) into Eqs. (24)–(26) gives the components of displacement, electric field, and strain in cylindrical coordinates, written as

$$\left.\begin{aligned}
u_r &= \sum_{i=1}^{2}\int_0^\infty \left\{\begin{array}{l} \sqrt{\mu_i}\alpha A_i(\alpha)\frac{1}{2}\left[I_0\left(\sqrt{\mu_i}\alpha r\right) + I_2\left(\sqrt{\mu_i}\alpha r\right)\right] \\ +\sqrt{\upsilon_i}\alpha C_i(\alpha)\frac{1}{2}\left[I_0\left(\sqrt{\upsilon_i}\alpha r\right) - I_2\left(\sqrt{\upsilon_i}\alpha r\right)\right] \end{array}\right\} \sin(\alpha z)\mathrm{d}\alpha \times \cos\theta, \\
u_\theta &= -\sum_{i=1}^{2}\int_0^\infty \left\{\begin{array}{l} \sqrt{\mu_i}\alpha A_i(\alpha)\frac{1}{2}\left[I_0\left(\sqrt{\mu_i}\alpha r\right) - I_2\left(\sqrt{\mu_i}\alpha r\right)\right] \\ +\sqrt{\upsilon_i}\alpha C_i(\alpha)\frac{1}{2}\left[I_0\left(\sqrt{\upsilon_i}\alpha r\right) + I_2\left(\sqrt{\upsilon_i}\alpha r\right)\right] \end{array}\right\} \sin(\alpha z)\mathrm{d}\alpha \times \sin\theta, \\
u_z &= \sum_{i=1}^{2}\int_0^\infty k_i\alpha A_i(\alpha) I_1\left(\sqrt{\mu_i}\alpha r\right)\cos(\alpha z)\mathrm{d}\alpha \times \cos\theta
\end{aligned}\right\}, \tag{32}$$

$$\left.\begin{aligned}
E_r &= \frac{c_{44}}{e_{14}\mu_3}\sum_{i=1}^{2}\int_0^\infty (\upsilon_i - \mu_3)\sqrt{\upsilon_i}\alpha^2 C_i(\alpha)\frac{1}{2}\left[I_0\left(\sqrt{\upsilon_i}\alpha r\right) + I_2\left(\sqrt{\upsilon_i}\alpha r\right)\right]\cos(\alpha z)\mathrm{d}\alpha \times \sin\theta, \\
E_\theta &= \frac{c_{44}}{e_{14}\mu_3}\sum_{i=1}^{2}\int_0^\infty (\upsilon_i - \mu_3)\sqrt{\upsilon_i}\alpha^2 C_i(\alpha)\frac{1}{2}\left[I_0\left(\sqrt{\upsilon_i}\alpha r\right) - I_2\left(\sqrt{\upsilon_i}\alpha r\right)\right]\cos(\alpha z)\mathrm{d}\alpha \times \cos\theta, \\
E_z &= -\frac{c_{44}}{e_{14}\mu_3}\sum_{i=1}^{2}\int_0^\infty (\upsilon_i - \mu_3)\alpha^2 C_i(\alpha) I_1\left(\sqrt{\upsilon_i}\alpha r\right)\sin(\alpha z)\mathrm{d}\alpha \times \sin\theta
\end{aligned}\right\}, \tag{33}$$

$$
\left.
\begin{aligned}
\varepsilon_{rr} &= \sum_{i=1}^{2} \int_0^{\infty} \left\{ \begin{array}{l} \mu_i \alpha^2 A_i(\alpha) \dfrac{1}{4} \left[3I_1\left(\sqrt{\mu_i}\alpha r\right) + I_3\left(\sqrt{\mu_i}\alpha r\right) \right] \\ +\upsilon_i \alpha^2 C_i(\alpha) \dfrac{1}{4} \left[I_1\left(\sqrt{\upsilon_i}\alpha r\right) - I_3\left(\sqrt{\upsilon_i}\alpha r\right) \right] \end{array} \right\} \sin(\alpha z) \mathrm{d}\alpha \times \cos\theta, \\
\varepsilon_{\theta\theta} &= \sum_{i=1}^{2} \int_0^{\infty} \left\{ \begin{array}{l} \mu_i \alpha^2 A_i(\alpha) \dfrac{1}{4} \left[I_1\left(\sqrt{\mu_i}\alpha r\right) - I_3\left(\sqrt{\mu_i}\alpha r\right) \right] \\ -\upsilon_i \alpha^2 C_i(\alpha) \dfrac{1}{4} \left[I_1\left(\sqrt{\upsilon_i}\alpha r\right) - I_3\left(\sqrt{\upsilon_i}\alpha r\right) \right] \end{array} \right\} \sin(\alpha z) \mathrm{d}\alpha \times \cos\theta, \\
\varepsilon_{zz} &= \sum_{i=1}^{2} \int_0^{\infty} \left(-k_i \alpha^2 \right) A_i(\alpha) I_1\left(\sqrt{\mu_i}\alpha r\right) \sin(\alpha z) \mathrm{d}\alpha \times \cos\theta, \\
2\varepsilon_{\theta z} &= -\sum_{i=1}^{2} \int_0^{\infty} \left\{ \begin{array}{l} (1+k_i)\sqrt{\mu_i} \alpha^2 A_i(\alpha) \dfrac{1}{2} \left[I_0\left(\sqrt{\mu_i}\alpha r\right) - I_2\left(\sqrt{\mu_i}\alpha r\right) \right] \\ +\sqrt{\upsilon_i} \alpha^2 C_i(\alpha) \dfrac{1}{2} \left[I_0\left(\sqrt{\upsilon_i}\alpha r\right) + I_2\left(\sqrt{\upsilon_i}\alpha r\right) \right] \end{array} \right\} \cos(\alpha z) \mathrm{d}\alpha \times \sin\theta, \\
2\varepsilon_{zr} &= \sum_{i=1}^{2} \int_0^{\infty} \left\{ \begin{array}{l} (1+k_i)\sqrt{\mu_i} \alpha^2 A_i(\alpha) \dfrac{1}{2} \left[I_0\left(\sqrt{\mu_i}\alpha r\right) + I_2\left(\sqrt{\mu_i}\alpha r\right) \right] \\ +\sqrt{\upsilon_i} \alpha^2 C_i(\alpha) \dfrac{1}{2} \left[I_0\left(\sqrt{\upsilon_i}\alpha r\right) - I_2\left(\sqrt{\upsilon_i}\alpha r\right) \right] \end{array} \right\} \cos(\alpha z) \mathrm{d}\alpha \times \cos\theta, \\
2\varepsilon_{r\theta} &= -2\sum_{i=1}^{2} \int_0^{\infty} \left\{ \begin{array}{l} \mu_i \alpha^2 A_i(\alpha) \dfrac{1}{4} \left[I_1\left(\sqrt{\mu_i}\alpha r\right) - I_3\left(\sqrt{\mu_i}\alpha r\right) \right] \\ +\upsilon_i \alpha^2 C_i(\alpha) \dfrac{1}{4} \left[I_1\left(\sqrt{\upsilon_i}\alpha r\right) + I_3\left(\sqrt{\upsilon_i}\alpha r\right) \right] \end{array} \right\} \sin(\alpha z) \mathrm{d}\alpha \times \sin\theta
\end{aligned}
\right\}. \tag{34}
$$

The components of the stress and electric displacement can be obtained by substituting Eqs. (33) and (34) into Eqs. (1) and (2), respectively, but are not written explicitly, here.

The electric potential distribution on the surface, $(\Phi)_{r=R}$, can be expressed in the Fourier integral form [20],

$$
(\Phi)_{r=R} = \Phi_0 \int_0^{\infty} f^*(\alpha) \cos(\alpha z) \mathrm{d}\alpha \times \sin\theta, \tag{35}
$$

where

$$
f^*(\alpha) = \frac{\delta}{\sqrt{\pi}} \exp\left(-\frac{\alpha^2 \delta^2}{4} \right). \tag{36}
$$

Equation (36) denotes the Fourier-cosine transform of the function $\exp\left(-z^2/\delta^2\right)$ in the last equation of Eq. (28). For a practical distribution with respect to z such as partially uniform one, the solution procedures are still valid by replacing Eq. (36) with the corresponding Fourier-cosine transform, which also suggests the versatility of our methodology. By substituting Eqs. (33) and (34) into Eq. (1) and the resulting equations, Eqs. (31), and (35) into Eq. (28), we determine a set of simultaneous equations for $A_i(\alpha)$ and $C_i(\alpha)$, (i =1, 2),

$$\left.\begin{aligned}
\sum_{i=1}^{2}\left\langle \alpha^2 A_i(\alpha)\left\{[\mu_3(1+k_i)-\mu_i]I_1\left(\sqrt{\mu_i}\alpha R\right)+2\mu_i\frac{1}{4}\left[I_1\left(\sqrt{\mu_i}\alpha R\right)+I_3\left(\sqrt{\mu_i}\alpha R\right)\right]\right\}\right.\\
\left.+2\upsilon_i\alpha^2 C_i(\alpha)\frac{1}{4}[I_1(\sqrt{\upsilon_i}\alpha R)-I_3(\sqrt{\upsilon_i}\alpha R)]\right\rangle=0,\\
\sum_{i=1}^{2}\left\{\begin{array}{l} 2\mu_i\alpha^2 A_i(\alpha)\frac{1}{4}\left[I_1\left(\sqrt{\mu_i}\alpha R\right)-I_3\left(\sqrt{\mu_i}\alpha R\right)\right]\\ +2\upsilon_i\alpha^2 C_i(\alpha)\frac{1}{4}[I_1(\sqrt{\upsilon_i}\alpha R)+I_3(\sqrt{\upsilon_i}\alpha R)]\end{array}\right\}=0,\\
\sum_{i=1}^{2}\left\{\begin{array}{l}(1+k_i)\sqrt{\mu_i}\alpha^2 A_i(\alpha)\frac{1}{2}\left[I_0\left(\sqrt{\mu_i}\alpha R\right)+I_2\left(\sqrt{\mu_i}\alpha R\right)\right]\\ +\frac{1}{\mu_3}\upsilon_i\sqrt{\upsilon_i}\alpha^2 C_i(\alpha)\frac{1}{2}[I_0(\sqrt{\upsilon_i}\alpha R)-I_2(\sqrt{\upsilon_i}\alpha R)]\end{array}\right\}=0,\\
\sum_{i=1}^{2}(\upsilon_i-\mu_3)\alpha^2 C(\alpha)\frac{I_1\left(\sqrt{\upsilon_i}\alpha R\right)}{\alpha}=-\frac{e_{14}\mu_3\Phi_0}{c_{44}}f^*(\alpha)
\end{aligned}\right\}. \tag{37}$$

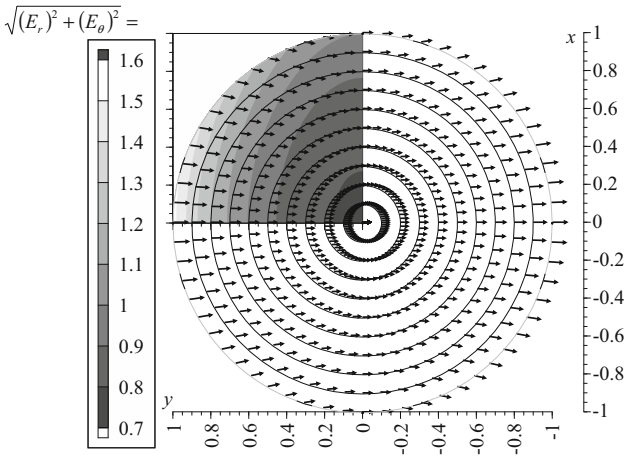

Fig. 3 Distribution of electric field vectors in the cylindrical cross section $(z=0)$

Equation (37) is solved as

$$\alpha^2\{A_1(\alpha)\quad A_2(\alpha)\quad C_1(\alpha)\quad C_2(\alpha)\}=-\frac{e_{14}\mu_3\Phi_0}{c_{44}}\frac{f^*(\alpha)}{\Delta(\alpha)}\{A_1^*(\alpha)\quad A_2^*(\alpha)\quad C_1^*(\alpha)\quad C_2^*(\alpha)\}, \tag{38}$$

where

$$
\left.
\begin{aligned}
\Delta(\alpha) &= \Delta_{12}(\alpha) + \Delta_{21}(\alpha),\\
\Delta_{ij}(\alpha) &= (1+k_i)I_1\left(\sqrt{\mu_i}\alpha R\right)\left\{\left[\mu_3(1+k_j)-\mu_j\right]I_1\left(\sqrt{\mu_j}\alpha R\right)+\mu_j I_3\left(\sqrt{\mu_j}\alpha R\right)\right\}\\
&\quad\times\left\{\begin{array}{l}(\upsilon_i-\mu_3)\upsilon_j\sqrt{\upsilon_j}\dfrac{I_1\left(\sqrt{\upsilon_i}\alpha R\right)}{\alpha}\left[I_0\left(\sqrt{\upsilon_j}\alpha R\right)-I_2\left(\sqrt{\upsilon_j}\alpha R\right)\right]\\ -\left(\upsilon_j-\mu_3\right)\upsilon_i\sqrt{\upsilon_i}\dfrac{I_1\left(\sqrt{\upsilon_j}\alpha R\right)}{\alpha}\left[I_0(\sqrt{\upsilon_i}\alpha R)-I_2(\sqrt{\upsilon_i}\alpha R)\right]\end{array}\right\}\\
&\quad+\sqrt{\mu_i}\mu_3(1+k_i)\left(1+k_j\right)I_1\left(\sqrt{\mu_j}\alpha R\right)\left[I_0\left(\sqrt{\mu_i}\alpha R\right)+I_2\left(\sqrt{\mu_i}\alpha R\right)\right]\\
&\quad\times\left[-(\upsilon_i-\mu_3)\upsilon_j\frac{I_1\left(\sqrt{\upsilon_i}\alpha R\right)I_3\left(\sqrt{\upsilon_j}\alpha R\right)}{\alpha}+\left(\upsilon_j-\mu_3\right)\upsilon_i\frac{I_1\left(\sqrt{\upsilon_j}\alpha R\right)I_3\left(\sqrt{\upsilon_i}\alpha R\right)}{\alpha}\right]\\
&\quad-(1+k_i)\sqrt{\mu_i}\left[I_0\left(\sqrt{\mu_i}\alpha R\right)+I_2\left(\sqrt{\mu_i}\alpha R\right)\right]\left\{\left[\mu_3(1+k_j)-\mu_j\right]I_1\left(\sqrt{\mu_j}\alpha R\right)+\mu_j I_3\left(\sqrt{\mu_j}\alpha R\right)\right\}\\
&\quad\times\left[(\upsilon_i-\mu_3)\upsilon_j\frac{I_1\left(\sqrt{\upsilon_i}\alpha R\right)I_1\left(\sqrt{\upsilon_j}\alpha R\right)}{\alpha}-\left(\upsilon_j-\mu_3\right)\upsilon_i\frac{I_1\left(\sqrt{\upsilon_j}\alpha R\right)I_1\left(\sqrt{\upsilon_i}\alpha R\right)}{\alpha}\right],\\
A_1^*(\alpha) &= \upsilon_1\upsilon_2(1+k_2)I_1\left(\sqrt{\mu_2}\alpha R\right)\\
&\quad\times\{-\sqrt{\upsilon_2}I_3(\sqrt{\upsilon_1}\alpha R)[I_0(\sqrt{\upsilon_2}\alpha R)-I_2(\sqrt{\upsilon_2}\alpha R)]+\sqrt{\upsilon_1}I_3(\sqrt{\upsilon_2}\alpha R)[I_0(\sqrt{\upsilon_1}\alpha R)-I_2(\sqrt{\upsilon_1}\alpha R)]\}\\
&\quad-\frac{1}{\mu_3}\upsilon_1\upsilon_2\left\{\left[\mu_3(1+k_2)-\mu_2\right]I_1\left(\sqrt{\mu_2}\alpha R\right)+\mu_2 I_3\left(\sqrt{\mu_2}\alpha R\right)\right\}\\
&\quad\times\{\sqrt{\upsilon_2}I_1(\sqrt{\upsilon_1}\alpha R)[I_0(\sqrt{\upsilon_2}\alpha R)-I_2(\sqrt{\upsilon_2}\alpha R)]-\sqrt{\upsilon_1}I_1(\sqrt{\upsilon_2}\alpha R)[I_0(\sqrt{\upsilon_1}\alpha R)-I_2(\sqrt{\upsilon_1}\alpha R)]\}\\
&\quad+\upsilon_1\upsilon_2(1+k_2)\sqrt{\mu_2}\left[I_0\left(\sqrt{\mu_2}\alpha R\right)+I_2\left(\sqrt{\mu_2}\alpha R\right)\right][-I_1(\sqrt{\upsilon_1}\alpha R)I_3(\sqrt{\upsilon_2}\alpha R)+I_1(\sqrt{\upsilon_2}\alpha R)I_3(\sqrt{\upsilon_1}\alpha R)],\\
C_1^*(\alpha) &= \upsilon_2 I_1(\sqrt{\upsilon_2}\alpha R)\left\langle\begin{array}{l}(1+k_2)\sqrt{\mu_2}\left\{\left[\mu_3(1+k_1)-\mu_1\right]I_1\left(\sqrt{\mu_1}\alpha R\right)+\mu_1 I_3\left(\sqrt{\mu_1}\alpha R\right)\right\}\left[I_0\left(\sqrt{\mu_2}\alpha R\right)+I_2\left(\sqrt{\mu_2}\alpha R\right)\right]\\ -(1+k_1)\sqrt{\mu_1}\left\{\left[\mu_3(1+k_2)-\mu_2\right]I_1\left(\sqrt{\mu_2}\alpha R\right)+\mu_2 I_3\left(\sqrt{\mu_2}\alpha R\right)\right\}\left[I_0\left(\sqrt{\mu_1}\alpha R\right)+I_2\left(\sqrt{\mu_1}\alpha R\right)\right]\end{array}\right\rangle\\
&\quad+\mu_3(1+k_1)(1+k_2)\upsilon_2 I_3(\sqrt{\upsilon_2}\alpha R)\left\{\begin{array}{l}\sqrt{\mu_2}I_1\left(\sqrt{\mu_1}\alpha R\right)\left[I_0\left(\sqrt{\mu_2}\alpha R\right)+I_2\left(\sqrt{\mu_2}\alpha R\right)\right]\\ -\sqrt{\mu_1}I_1\left(\sqrt{\mu_2}\alpha R\right)\left[I_0\left(\sqrt{\mu_1}\alpha R\right)+I_2\left(\sqrt{\mu_1}\alpha R\right)\right]\end{array}\right\}\\
&\quad+\upsilon_2\sqrt{\upsilon_2}[I_0(\sqrt{\upsilon_2}\alpha R)-I_2(\sqrt{\upsilon_2}\alpha R)]\left\{\begin{array}{l}\mu_2(1+k_1)I_1\left(\sqrt{\mu_1}\alpha R\right)\left[-I_1\left(\sqrt{\mu_2}\alpha R\right)+I_3\left(\sqrt{\mu_2}\alpha R\right)\right]\\ -\mu_1(1+k_2)I_1\left(\sqrt{\mu_2}\alpha R\right)\left[-I_1\left(\sqrt{\mu_1}\alpha R\right)+I_3\left(\sqrt{\mu_1}\alpha R\right)\right]\end{array}\right\}
\end{aligned}
\right\}. \tag{39}
$$

$A_2^*(\alpha)$ and $C_2^*(\alpha)$ are defined identically to $A_1^*(\alpha)$ and $C_1^*(\alpha)$, respectively, but with subscripts "1" and "2" interchanged for k_i, μ_i, and υ_i. By substituting Eqs. (38) and (39) into Eqs. (1), (2), and (31)–(34), we formulate the electroelastic field quantities in cylindrical coordinates.

Resultant forces and moments in cylindrical cross section

When we assume an NDE, not only the detail distributions of electroelastic field quantities but also the overall behavior of the quantities needs to be elucidated because it is related to supporting conditions for a specimen. Motivated by this idea, we investigate the resultant effects of stresses in the cross section perpendicular to the z-axis by the resultant forces in the x, y, and z directions and the resultant moments around the x-, y-, and z-axes, respectively, defined as

$$
\begin{aligned}
\left(N_x, N_y, N_z\right) &= \int_{S_z}\left(\sigma_{zx}, \sigma_{yz}, \sigma_{zz}\right)\mathrm{d}S_z,\\
\left(M_x, M_y, M_z\right) &= \int_{S_z}\left(y\sigma_{zz}, -x\sigma_{zz}, r\sigma_{\theta z}\right)\mathrm{d}S_z,
\end{aligned} \tag{40}
$$

where σ_{zx} and σ_{yz} denote the components of stress in the Cartesian coordinate system (x, y, z) and $\mathrm{d}S_z$ denotes a small elemental area of the cylindrical cross section S_z. By

substituting Eqs. (33) and (34) into Eq. (1), and applying the coordinate transformation

$$\sigma_{zx} = \sigma_{zr}\cos\theta - \sigma_{\theta z}\sin\theta,\ \ \sigma_{yz} = \sigma_{zr}\sin\theta + \sigma_{\theta z}\cos\theta, \tag{41}$$

we arrived at expressions for Cartesian stresses. In light of the symmetry of stresses with respect to $x = 0$ and $y = 0$, integrating these stresses in Eq. (40) resulted in

$$\left.\begin{aligned} N_x &= c_{44}\sum_{i=1}^{2}\left\{\int_0^\infty \pi\alpha R\left[(1+k_i)A_i(\alpha)I_1\left(\sqrt{\mu_i}\alpha R\right) + \frac{1}{\mu_3}\upsilon_i C_i(\alpha)I_1\left(\sqrt{\upsilon_i}\alpha R\right)\right]\cos(\alpha z)\mathrm{d}\alpha\right\},\\ M_y &= c_{44}\sum_{i=1}^{2}\left\{\int_0^\infty \pi(1+k_i)A_i(\alpha)\left[\sqrt{\mu_i}\alpha R^2 I_0\left(\sqrt{\mu_i}\alpha R\right) - 2RI_1\left(\sqrt{\mu_i}\alpha R\right)\right]\sin(\alpha z)\mathrm{d}\alpha\right\},\\ N_y &= N_z = 0,\ \ M_x = M_z = 0 \end{aligned}\right\}. \tag{42}$$

However, by the first and second equations in Eq. (37),

$$N_x = 0 \tag{43}$$

for any value of z. $\left(M_y\right)_{z=0} = 0$ from Eq. (42) and the cylindrical surface was free from stresses, as prescribed in Eq. (28). Therefore, by considering an equilibrium of the resultant forces and moments in the free body between $z = 0$ and S_z, the resultant moment around the y-axis is

$$M_y = 0 \tag{44}$$

for any value of z. Thus, from Eqs. (42)–(44), the cylindrical cross section, S_z, is free from the resultant forces and moments for any value of z, including $z \to \infty$, although boundary conditions in the cylindrical cross section were not explicitly prescribed in Eq. (28). Meanwhile, from the viewpoint of mechanical design, these results imply that considering the resultant effects only leads to an oversight of the stresses which may cause the undesired failures, and again evoke the necessity for the detail analysis of electroelastic field quantities, which is presented in the following subsection.

Numerical calculations

As the piezoelectric body, Sitka spruce (*Picea sitchensis*) is chosen. The material properties are given by

$$\left.\begin{aligned} c_{11} &= 830.84\,[\mathrm{MPa}],\ c_{33} = 12.276\,[\mathrm{GPa}],\ c_{12} = 294.47\,[\mathrm{MPa}],\\ c_{13} &= 472.07\,[\mathrm{MPa}],\ c_{44} = 742.50\,[\mathrm{MPa}],\\ \eta_{11} &= 16.823\times10^{-12}\left[\frac{\mathrm{C}^2}{\mathrm{N}\times\mathrm{m}^2}\right],\ \eta_{33} = 22.490\times10^{-12}\left[\frac{\mathrm{C}^2}{\mathrm{N}\times\mathrm{m}^2}\right],\ e_{14} = -0.14850\times10^{-3}\left[\frac{\mathrm{C}}{\mathrm{m}^2}\right] \end{aligned}\right\}, \tag{45}$$

for which μ_1 and μ_2 are different positive numbers. The construction of Eq. (45) is described in detail in our previous work [17], in which the set of material constants was constructed using data under various conditions because a complete set was not found under a common condition. The material constants generally depend on conditions such as moisture content, temperature and frequencies of mechanical and electrical loadings, which suggests the potential necessity for the coupling analysis with hygrothermal field and the dynamic

analysis. In this paper, however, the values in Eq. (45) are chosen as a first step to solve the problems in cylindrical bodies with D_∞ symmetry. To illustrate the numerical results, the following nondimensional quantities were introduced:

$$\left.\begin{aligned}\left(\widehat{r},\widehat{z},\widehat{\delta}\right)\equiv\frac{(r,z,\delta)}{R},\ \left(\widehat{c}_{11},\widehat{c}_{12},\widehat{c}_{13},\widehat{c}_{33}\right)\equiv\frac{(c_{11},c_{12},c_{13},c_{33})}{c_{44}},\ \widehat{u}_i\equiv\frac{u_i}{|e_{14}|\Phi_0/c_{44}},\\ \widehat{\varepsilon}_{ij}\equiv\frac{\varepsilon_{ij}}{|e_{14}|\Phi_0/(c_{44}R)},\ \widehat{E}_i\equiv\frac{E_i}{\Phi_0/R},\ \widehat{\sigma}_{ij}\equiv\frac{\sigma_{ij}}{|e_{14}|\Phi_0/R}\ (i,j=r,\theta,z,x,y)\end{aligned}\right\}. \tag{46}$$

The effective width of the distribution along the z-axis was assumed to be

$$\widehat{\delta}=1. \tag{47}$$

For brevity, we hereafter omit the signs for nondimensional quantities in Eq. (46), $\widehat{\ }$.

Figures 3, 4 and 5 show the distributions of electric field vectors, vector expressions of the maximum shear strain, and shear stress vectors, respectively, in the cylindrical cross section at $z=0$, where E_z, ε_{zz}, and σ_{zz} vanish from Eqs. (1), (33), and (34). In Figs. 3, 4 and 5, the x- and y-axes are oriented for comparison with the right panel of Fig. 2. The directions and relative vector magnitudes are indicated by the directions and lengths of arrows, and the absolute magnitudes $\sqrt{(E_r)^2+(E_\theta)^2}$, $\sqrt{(2\varepsilon_{zr})^2+(2\varepsilon_{\theta z})^2}$, and $\sqrt{(\sigma_{zr})^2+(\sigma_{\theta z})^2}$ are indicated by contours in the upper left quadrants.

In Fig. 3, the electric field is directed mainly in the $-y$ direction, so as to reflect the nature of electric boundary condition illustrated in Fig. 2 and prescribed by Eq. (28). The magnitude of the electric field is greater near the electrically-loaded surfaces, $\theta\cong\pm\pi/2$ and $r\cong1$, than in the core, $r\cong0$. Figure 4 shows the shear deformation is primarily in $-x$ direction, reflecting the nature of D_∞ symmetry illustrated in Fig. 1 in conjunction with the negative piezoelectric coefficient of Eq. (45). As shown in Figs. 3 and 4, the magnitude of the maximum shear strain exhibits a distribution similar to that of the electric field.

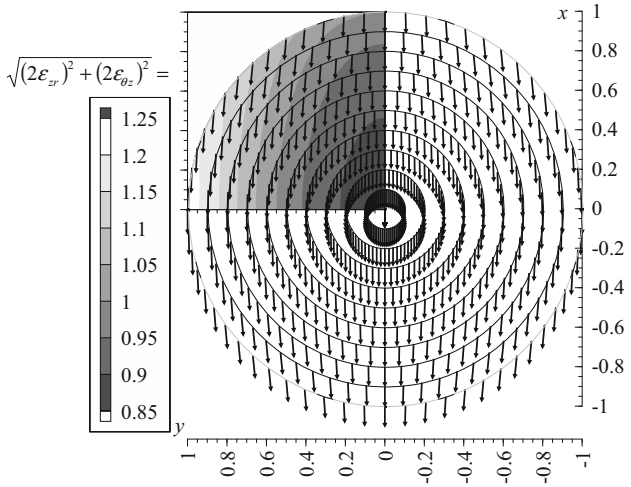

Fig. 4 Distribution of vector expressions of maximum shear strain in the cylindrical cross section ($z=0$)

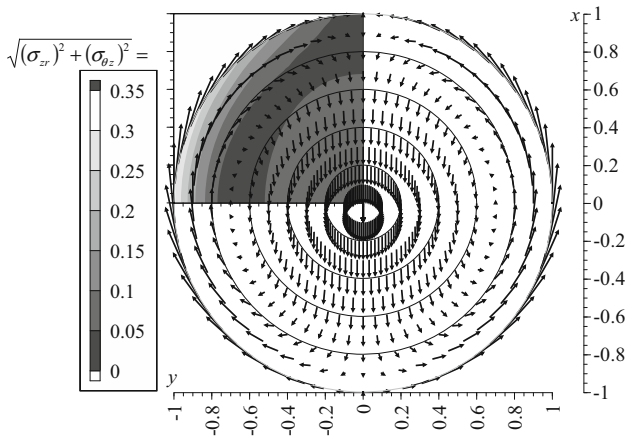

Fig. 5 Distribution of shear stress vectors in the cylindrical cross section ($z=0$)

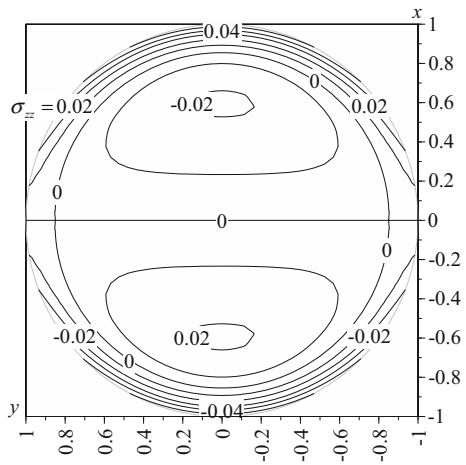

Fig. 6 Distribution of axial stresses in the cylindrical cross section ($z=1$)

Unlike the electric field and shear strain shown in Figs. 3 and 4, the shear stress exhibits a somewhat complicated distribution, as shown in Fig. 5. Due to the antisymmetry of the surface electric potential described by Eq. (27), the shear stresses in the y and θ directions cancel each other out around $y = 0$; therefore, the resultant shear force in y direction, N_y, and the resultant twisting moment around z-axis, M_z, are absent, as predicted by Eq. (42). On the other hand, because the shear stress in the x direction is symmetric to either side of $x = 0$, as shown in Fig. 5, the resultant shear force in the x direction, N_x, is likely nonzero. However, as shown in Fig. 5, because the direction of the shear stress σ_{zx} is inverted in the core and skin regions, the shear stresses in both regions cancel each other out, so the resultant shear force in the x direction, N_x, vanishes, as in Eq. (43). An important aspect obtained from Fig. 5 is that considering the resultant forces and moments only leads to an oversight of the stresses which may break constituent molecular chains and that the detail analysis of electroelastic field quantities is absolutely essential.

We investigated the effects of the axial stress in the cylindrical cross section, σ_{zz}, on the resultant axial force, N_z, and the resultant bending moments, M_x and M_y defined by Eq. (40). For $z = 0$, the value of σ_{zz} vanishes, as found from Eqs. (1) and (34), making this case trivial. Therefore, we investigated the effects at $z = 1$. As shown in Fig. 6, because the direction of the axial stress σ_{zz} is antisymmetric around $x = 0$, the resultant axial force in the z direction, N_z, is absent, as predicted in Eq. (42). Similarly, because the distribution of stress σ_{zz} is symmetric around $y = 0$, the resultant bending moment around the x-axis, M_x, is absent, as predicted in Eq. (42). On the other hand, because the stress σ_{zz} is distributed anti-symmetrically around $x = 0$, the resultant bending moment around the y-axis, M_y, is likely nonzero. However, because the direction of stress σ_{zz} is inverted in the core and skin regions, as seen in the upper semicircle in Fig. 6, the resultant bending moment around the y-axis, M_y, vanishes, as predicted in Eq. (44). An important aspect obtained from Fig. 6 is that, although the cylinder are curved by the electric field as will be explained later (Fig. 7), the behaviors cannot be investigated by the bending moment, which also demonstrates the necessity for the detail analysis of electroelastic field quantities.

Then, we investigated the overall deformation behavior. Figure 8 shows the variations of the main component of electric field, $-E_y$, and that of shear strain, $-2\varepsilon_{zx}$, with axial position. From Fig. 8, the magnitude of $-E_y$ is maximum at $z = 0$ and decreases towards zero with increasing z, mirroring the surface electric potential distribution described by Eq. (27). The variation of $-2\varepsilon_{zx}$ with

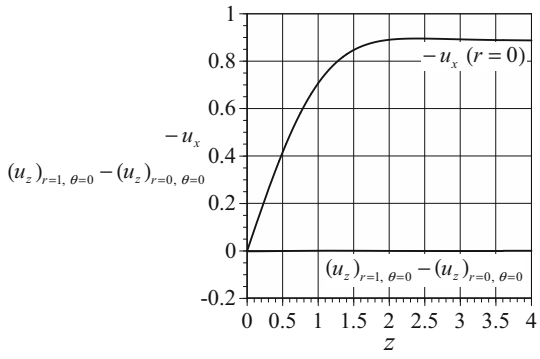

Fig. 7 Variations of displacement and displacement gradient with the axial location

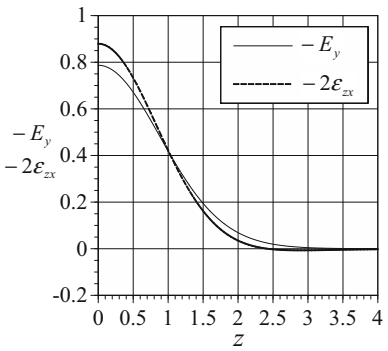

Fig. 8 Variations of the main components of electric field and shear strain with axial location $(r = 0)$

the axial position is similar to that of $-E_y$, reflecting the D_∞ symmetry illustrated in Fig. 1 along with the negative piezoelectric coefficient in Eq. (45). Figure 7 shows the variation of the displacement in the $-x$ direction, $-u_x$, resulting from the shear strain $-2\varepsilon_{zx}$ with axial position. From Fig. 7, the magnitude of the displacement is zero at $z = 0$, increases with z, and converges to a constant value after a subtle overshoot. Figure 7 also shows the variation of the average gradient of the axial displacement with respect to the radial coordinate, namely $(u_z)_{r=1,\,\theta=0} - (u_z)_{r=0,\,\theta=0}$. From Fig. 7, the gradient $(u_z)_{r=1,\,\theta=0} - (u_z)_{r=0,\,\theta=0}$ is negligible compared with the gradient $(\partial u_x/\partial z)_{r=0}$. In other words, the cylindrical cross section perpendicular to the undeformed axis of the cylinder remains almost planar and perpendicular to the undeformed axis after deformation, quite unlike the bending of a Bernoulli–Euler beam [21]. This finding clearly demonstrates that the electrically driven deformation of a beam-like body with D_∞ symmetry cannot be analyzed as

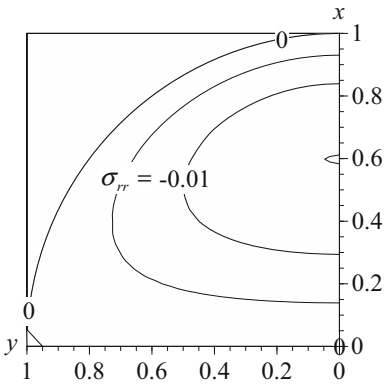

Fig. 9 Distribution of radial stresses in the cylindrical cross section ($z = 1$)

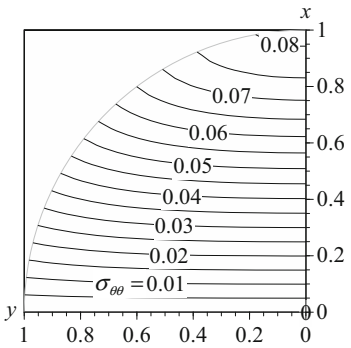

Fig. 10 Distribution of hoop stresses in the cylindrical cross section ($z = 1$)

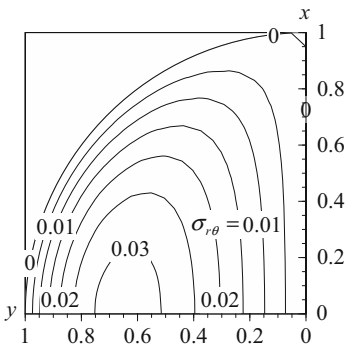

Fig. 11 Distribution of in-plane shear stresses in the cylindrical cross section ($z = 1$)

a Bernoulli–Euler beam and requires the three-dimensional analytical technique presented in this paper.

Finally, we examined the detection of information within the body. Figures 9, 10 and 11 show the distributions of in-plane stress components σ_{rr}, $\sigma_{\theta\theta}$, and $\sigma_{r\theta}$, respectively, in the cylindrical cross section at $z = 1$. These components are the possible causes of debonding between

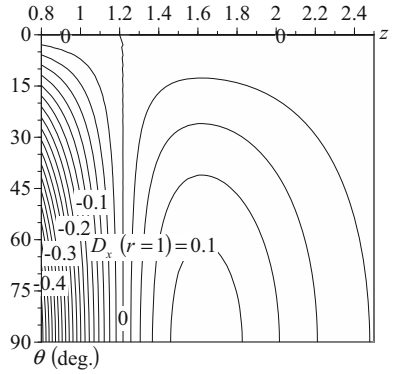

Fig. 12 Distribution of radial electric displacements on the surface ($r = 1$)

adjacent molecular chains, which in turn causes material defects such as cracks and voids. Conversely, these components are affected by such defects. These statements hold true also for σ_{zr}, $\sigma_{\theta z}$, and σ_{zz}, treated above: they are the possible causes of breakage of molecular chains in the cylindrical section, and are affected by the defects due to such breakage. In other words, the changes in stress components are closely related to the existence of defects. In an NDE, the changes in these quantities must be detected as measurable signals. From this viewpoint, the distribution of electric displacement in the radial direction, D_r, on the surface $r = 1$ is investigated. As shown in Fig. 12, the electric displacement is developed not only in the effective region of the surface electric potential, e.g. $z < 1.2$, but also in the remaining region, e.g. $z > 1.2$. Such a subsidiary electric displacement, which can be detected by a charge amplifier, is a candidate for the signal that reflects the information within the body, which should be examined in future research.

Concluding remarks

We constructed a general solution technique for electroelastic problems in bodies with D_∞ symmetry in the framework of a cylindrical coordinate system. The electroelastic field quantities could be expressed in terms of four functions, namely, two elastic displacement potential functions and two piezoelastic displacement potential functions, each of which satisfies a Laplace equation with respect to the appropriately transformed cylindrical coordinates. Moreover, as an application of the technique, we analyzed the problem of an infinitely long cylinder subjected to a non-axisymmetrical electric potential on its surface and illustrated the results graphically. We elucidated the behaviors of the electroelastic field quantities within the body, which cannot be measured

experimentally, and illustrated the necessity for the three-dimensional analytical technique presented in this paper. Moreover, we confirmed the possibility of the NDE techniques by use of the piezoelectric effects.

References

1. Fukada E (1955) Piezoelectricity of wood. J Phys Soc Jpn 10:149–154
2. Galligan WL, Bertholf LD (1963) Piezoelectric effect in wood. For Prod J 13:517–524
3. Smetana JA, Kelso PW (1971) Piezoelectric charge density measurements on the surface of Douglas-fir. Wood Sci 3:161–171
4. Knuffel W, Pizzi A (1986) The piezoelectric effect in structural timber. Holzforsch 40:157–162
5. Knuffel WE (1988) The piezoelectric effect in structural timber—part II. The influence of natural defects. Holzforsch 42:247–252
6. Nakai T, Igushi N, Ando K (1998) Piezoelectric behavior of wood under combined compression and vibration stresses I: relation between piezoelectric voltage and microscopic deformation of a Sitka spruce (*Picea sitchensis Carr.*). J Wood Sci 44:28–34
7. Nakai T, Ando K (1998) Piezoelectric behavior of wood under combined compression and vibration stresses II: effect of the deformation of cross-sectional wall of tracheids on changes in piezoelectric voltage in linear-elastic region. J Wood Sci 44:255–259
8. Nakai T, Hamatake M, Nakao T (2004) Relationship between piezoelectric behavior and the stress—strain curve of wood under combined compression and vibration stresses. J Wood Sci 50:97–99
9. Nakai T, Yamamoto H, Hamatake M, Nakao T (2006) Initial shapes of stress-strain curve of wood specimen subjected to repeated combined compression and vibration stresses and the piezoelectric behavior. J Wood Sci 52:539–543
10. Ishihara K, Sobue N, Takemura T (1978) Effect of grain angle on complex Young's modulus E^* of Spruce and Hoo. Mokuzai Gakkaishi 24:375–379
11. Sobue N, Asano I (1976) Studies on the fine structure and mechanical properties of wood–on the longitudinal Young's modulus and shear modulus of rigidity of cell wall (in Japanese). Mokuzai Gakkaishi 22:211–216
12. Norimoto M (1976) Dielectric properties of wood. Wood Res Bull Wood Res Inst Kyoto Univ 59–60:106–152
13. Norimoto M, Hayashi S, Yamada T (1978) Anisotropy of dielectric constant in coniferous wood. Holzforsch 32:167–172
14. Hirai N, Asano I, Sobue N (1973) Piezoelectric anisotropy of wood (in Japanese). J Soc Mater Sci Jpn 22:948–955
15. Kim SK (1999) Group theoretical methods and applications to molecules and crystals. Cambridge University Press, Cambridge
16. Hirai N, Sobue N, Date M (2011) New piezoelectric moduli of wood: d_{31} and d_{32}. J Wood Sci 57:1–6
17. Ishihara M, Ootao Y, Kameo Y (2015) Analytical technique for electroelastic field in piezoelectric bodies belonging to point group D_∞. J Wood Sci 61:270–284
18. Ishihara M, Ootao Y, Kameo Y (2015) Electroelastic response of a piezoelectric semi-infinite body with D_∞ symmetry to surface friction. Int J Eng Res Appl 5(6–2):26–32
19. Noda N, Hetnarski RB, Tanigawa Y (2003) Thermal stresses, 2nd edn. Taylor & Francis, New York
20. Sneddon IN (1972) The use of integral transforms. McGraw-Hill, New York
21. Timoshenko S (1955) Strength of materials, part I, elementary theory and problems, 3rd edn. D. Van Nostrand Company, New York